https://doi.org/10.1144/jgs2023-195 | Vol. 181 | 2024 | jgs2023-195

Redox changes in the Iapetus Ocean during the Late Ordovician extinction crises



Alejandra Sánchez-Roda*, Paul B. Wignall, Yijun Xiong and Simon W. Poulton

School of Earth and Environment, University of Leeds, Leeds LS2 9JT, UK

B AS-R, 0009-0009-7184-1361; PBW, 0000-0001-8592-0305; SWP, 0000-0001-7621-189X

*Correspondence: alejandra.sanchez.roda@upc.edu

Abstract: The cause of the Late Ordovician mass extinction (LOME) is widely debated, with glaciation, volcanism and oceanic redox fluctuations being proposed as possible drivers. Here, we apply a multi-proxy approach to deep-water Iapetus Ocean samples from Dob's Linn, Scotland, to determine oceanic redox conditions and changes in chemical weathering intensity. We document major redox fluctuations between anoxic ferruginous and oxic conditions during the first, end-Katian extinction pulse, whereas the end-Hirnantian extinction phase witnessed more persistent anoxia. These two episodes were separated by oxic conditions and a major, short-lived decline in chemical weathering during the Hirnantian glaciation, suggesting that although global cooling may have placed stress on certain biota, it was unlikely to be the cause of the extinction crisis. Late Hirnantian anoxia persisted into the Silurian, with widespread euxinia resulting in global drawdown of redox-sensitive trace metals. Recent studies have identified a mid-Katian biotic crisis and recovery prior to the LOME, although the precise stratigraphic position is not yet defined. The mid-Katian record at Dob's Linn shows a major redox change, with dysoxic to anoxic ferruginous deep ocean waters giving way to well-oxygenated conditions at this time. However, links between the mid-Katian biotic crisis and these redox changes remain unclear.

Supplementary material: Supplementary tables are available at https://doi.org/10.6084/m9.figshare.c.7315858

Thematic collection: This article is part of the Chemical Evolution of the Mid-Paleozoic Earth System and Biotic Response collection available at: https://www.lyellcollection.org/topic/collections/chemical-evolution-of-the-mid-paleozoic-earth-system

Received 3 November 2023; revised 4 June 2024; accepted 5 June 2024

The Late Ordovician mass extinction (LOME) marks the first of the 'big five' crises to afflict animal life in the oceans. Extinction losses occurred in two major pulses during the Hirnantian, the final stage of the Ordovician, with the first (LOME-1) occurring around the base of the Metabolograptus extraordinarius graptolite zone, and the second (LOME-2) occurring within the succeeding M. persculptus Zone (Hallam and Wignall 1997; Sheehan 2001; Harper et al. 2014). Losses during LOME-1 were especially severe amongst deep shelf benthos and pelagic graptolites (Harper et al. 2014). LOME-2 was possibly a less severe crisis (Wang et al. 2019), but it again affected a broad range of groups in diverse habitats, with notable losses amongst the nektonic conodonts and the planktonic acritarchs (Brenchley and Štorch 1989; Brenchley et al. 1994; Harper et al. 2014). Recent studies have suggested that there was an earlier extinction crisis in the Katian, but it is currently unclear if losses were spread throughout the final 4-5 Myr of this stage (Rasmussen et al. 2019; Wang et al. 2019) or if there was a shorter, sharper extinction pulse (Deng et al. 2021). Based on a large, highresolution database from China, Deng et al. (2021) found that diversity began a rapid decline in the mid-Katian (448.7 Ma) and began to rise again in the latest Katian. If these trends are replicated globally then it suggests that there was a discrete mid-Katian extinction crisis, followed by recovery before the LOME crises.

The Late Ordovician was clearly a difficult time for marine life, and by the earliest Silurian species diversity had reduced to less than half its Katian value (Fan *et al.* 2020). The Late Ordovician was also a time of major climatic and environmental change, with several potential drivers being proposed for the extinctions. LOME-2 coincides with the onset of black shale deposition in many regions, and there is a broad consensus that this mass extinction phase was

caused by the spread of anoxia (e.g. Hallam and Wignall 1997; Brenchley et al. 2001; Zou et al. 2018a, b; Bond and Grasby 2020; Stockey et al. 2020; Dahl et al. 2021; Wang et al. 2022), although other studies suggest that different factors, in particular cooling, were more important (Pohl et al. 2021). By contrast, LOME-1 has traditionally been linked to global cooling and the onset of a short but intense glaciation in the southern hemisphere, the Hirnantian glaciation (Berry and Wilde 1978; Stanley 1988; Hallam and Wignall 1997). However, more recent studies, especially from South China, have suggested that the first crisis was also associated with the spread of anoxic waters immediately prior to the cooling event (Zhang et al. 2009; Zou et al. 2018b; Dahl et al. 2021; Wang et al. 2022). There is further debate concerning the role of changing nutrient levels both as a driver of these oceanic redox changes and as an additional cause of the extinctions (Armstrong and Harper 2014; Bond and Grasby 2020; Pohl et al. 2021; Qiu et al. 2022; Wang et al. 2022). Nutrient-driven expansion of continental margin oxygen minimum zones is favoured by some studies (Hammarlund et al. 2012; Longman et al. 2021; Qiu et al. 2022), whereas other studies highlight the possible role of a productivity crash, with warmer temperatures and decreased gas solubility leading to expanded ocean anoxia (Bond and Grasby 2020; Kozik et al. 2022).

Here, we aim to address the diverse debates regarding redox changes and the locus of black shale deposition, carbon isotope fluctuations, and the causes of the multiple extinction crises of the Late Ordovician, with an analysis from an open ocean location. Few abyssal sites are available for study in the Early Paleozoic, but here we argue that the celebrated section at Dob's Linn in Scotland provides a highly condensed, abyssal record from the Iapetus Ocean. We provide an integrated assessment of redox (iron speciation

systematics, redox-sensitive trace element (RSTE) data) and weathering proxies (chemical index of alteration; CIA), alongside the $\delta^{13}C_{org}$ record. Previous studies at Dob's Linn have focused on the Ordovician–Silurian transition (e.g. Bond and Grasby 2020), but here we expand the coverage to evaluate conditions during both LOME pulses and the earlier, little-studied mid-Katian crisis.

Study section and palaeogeographic context

Dob's Linn (Southern Uplands, Scotland, 55°25′46.484″N, 3°16′17.605′′W) is the Global Stratotype Section and Point (GSSP) for the Ordovician–Silurian boundary (Fig. 1). The section occurs within the accretionary prism that formed at the Laurentian margin as the Iapetus Ocean was destroyed during the Ordovician and Silurian (Strachan 2012). The stratigraphy belongs to the Moffatt Shale Group and consists of three formations: the Lower Hartfell Shale, a mid-Katian black shale; the Upper Hartfell Shale, a late Katian to early Hirnantian pale mudstone-dominated unit; and the Birkhill Shale, a late Hirnantian to early Llandovery black shale. Graptolites are abundant in the black shale-dominated formations, where they provide high-resolution biostratigraphy, but are restricted to thin beds of black shale, termed *Anceps* Bands, in the uppermost Upper Hartfell Shale (Williams 1988).

The Ordovician-Silurian boundary is fixed at 1.6 m above the base of the Birkhill Shale Formation, based on the first appearance of Parakidograptus acuminatus, and a thin succession of Hirnantian strata that straddle the Upper Hartfell Shale-Birkhill Shale boundary occurs beneath (Williams 1988). The base of the underlying M. persculptus Zone is placed in a thin black shale c. 60 cm below this formational boundary, based on the presence of the zonal graptolite (Mitchell and Melchin 2020). Metabolograptus extraordinarius also occurs at this level, which was termed the Extraordinarius Band by Williams (1988). The base of the M. extraordinarius Zone is not precisely known, but the eponymous graptolite also occurs lower down in the uppermost Anceps Band (Band E of Williams 1988) making this the likely level of the zonal boundary. However, Mitchell and Melchin (2020) placed the base of the M. extraordinarius Zone lower still, around the level of Anceps Band D, because of purported sedimentological evidence for the onset of the Hirnantian glaciation at this level. However, as we show below, there is clear geochemical evidence that the glaciation occurred at a higher level in the Hirnantian strata (above the Extraordinarius Band). We therefore place the base of the Hirnantian at Anceps Band E, thereby using graptolites to define graptolite zones, making the entire Hirnantian only 2.8 m thick.

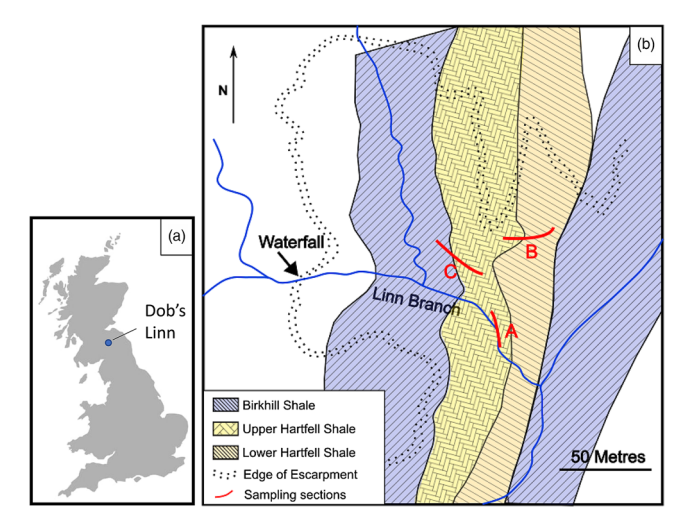


Fig. 1. Map of the location of sampled sections at Dob's Linn, Scotland, UK. (a) Location of Dob's Linn in the UK; (b) geological map of the area with the sampling points shown.

The depositional setting of the Moffat Shale Group at Dob's Linn has been ascribed either to the slope margin of the Laurentian continent (Hammarlund et al. 2012; Armstrong and Harper 2014; Bond and Grasby 2020; Dahl et al. 2021) or to a much more distal, abyssal plain setting within the Iapetus Ocean (Leggett 1978; Melchin et al. 2013; Stone 2014). Much of the associated Ordovician-Silurian geology of the Southern Uplands consists of thick, turbiditic sandstone successions typical of strata encountered in subduction trenches (Strachan 2012). By contrast, the Dob's Linn GSSP strata consist of fine-grained, highly condensed mudrocks typical of the Paleozoic ocean plain (Leggett 1978). The Geologic Time Scale 2020 gives durations of 7.54 Myr for the Katian and 2.14 Myr for the Hirnatian (Goldman et al. 2020), which produces compacted sediment accumulation rates of c. 5 and c. 1.5 mm ka⁻¹ for these respective stages at Dob's Linn. Such low sedimentation rates are typical of abyssal plains but are unlikely to be encountered in continental margin settings, especially one receiving large volumes of turbiditic sediment. The composition of the sediments is also characteristic of abyssal plain sediments (see below). Thus, we consider the Dob's Linn section to record ultra-condensed deposition in an open ocean setting, making it a rare archive of Ordovician-Silurian deep oceanic conditions. The section was subsequently obducted into the accretionary prism of the Southern Upland during the Late Silurian closure of the Iapetus Ocean (Leggett 1978; Stone 2014). Palaeogeographically, the Iapetus Ocean occurred in mid-latitudes in the southern hemisphere and was probably around 1500 km wide in the Katian, before narrowing to 500 km in the Early Silurian. Throughout this interval, the Iapetus Ocean maintained an open connection to the Panthalassic Ocean in the north, and to the Rheic Ocean in the SW (Cocks and Torsvik 2021).

Methods

Samples

A total of 74 mudstone and black shale samples were collected at Dob's Linn (Fig. 1). The stratigraphy is disrupted by numerous faults, resulting in only short sections of continuous stratigraphy being logged and sampled. Thus, 12 samples were taken from section A, a streamside section of the Upper Hartfell Shale, 25 samples were taken from section B (Lower Hartfell Shale) and 37 samples were taken from section C (Upper Hartfell Shale–Birkhill Shale), from the adjacent northern hillside (Fig. 1). The resultant composite section has a gap of c. 7.5 m within the Upper Hartfell Shale, based on comparison with the log of Williams (1988). Samples were analysed at the University of Leeds, where weathered or oxidized surfaces were removed using a diamond-tipped circular saw. The cleaned samples were then crushed and powdered using an agate tema mill.

Carbon concentrations and isotopes

Total organic carbon (TOC) and total carbon (TC) were determined on a LECO C-S analyser. Prior to analysis of TOC, carbonate phases were removed from the samples via two sequential dissolutions with 20% HCl. Samples were then washed with Milli-Q water to remove all the remaining acid and dried at 50°C. Reference materials (soil: 2.30 ± 0.06 wt% carbon content; soil LECO Certified Reference Material: 0.717 ± 0.027 wt% carbon content) were used for the calibration of the LECO and as internal standards. Replicate extractions gave a relative standard deviation (RSD) of <1%, and measurements were within 2% of certified values. Total inorganic carbon (TIC) was calculated as the difference between TC and TOC. Organic carbon isotopes were determined using a GB Isoprime mass spectrometer coupled to an Elementar Pyrocube, using the same samples as those prepared for TOC. Analyses were measured relative to CO2 reference gas, and results are given in δ notation

calibrated to the Vienna-Pee Dee Belemite (V-PDB) scale using urea and sucrose laboratory standards of known and calibrated isotopic composition (urea by Merck with $\delta^{13}C_{org}=-46.83\pm0.22\%$; Silver Spoon sucrose (commercial) with $\delta^{13}C_{org}=-26.19\pm0.10\%$; T&L sucrose (commercial) with $\delta^{13}C_{org}=-11.93\pm0.24\%$). Standard reproducibility given by repeat analyses of the internal sucrose standard was better than 0.1%.

Fe speciation

Iron speciation analyses were performed following the method of Poulton and Canfield (2005). First, iron carbonate phases (Fe_{carb}) were targeted using a Na-acetate solution at pH 4.5 and 50°C for 48 h. Then, ferric (oxyhydr)oxides (Fe_{ox}) were extracted using Na-dithionite solution at room temperature for 2 h. Finally, an ammonium oxalate solution was applied for 6 h at room temperature to target magnetite (Fe_{mag}). The concentration of all iron phases was determined using a Thermo Scientific iCE-3300 atomic absorption spectrometer. Pyrite (Fe_{py}) was extracted using a two-step chromous chloride distillation (Canfield et al. 1986), where the liberated sulfide was trapped as Ag₂S and the concentrations of sulfide were determined gravimetrically. In this procedure, acid volatile sulfide (AVS) was also determined, but in all cases was below detection. Replicate extractions of an international reference material (WHIT) gave an RSD of <5% for all Fe phases (Alcott et al. 2020). The highly reactive Fe fraction (FeHR) was calculated as the sum of $Fe_{carb}, Fe_{ox}, Fe_{mag}$ and Fe_{py} (Poulton and Canfield 2005). Total iron (Fe_T) was determined via the same procedure as other major elements (see below). Accuracy was monitored using the international reference material SBC-1, with Fe_T data being within 0.12% of certified values.

Major elements and trace metals

Samples were prepared for major and trace metal analyses via total digestion, which comprised ashing at 550°C for 8 h, followed by dissolution using a combination of concentrated HNO₃, HF and HClO₄, with boric acid used to prevent the formation of Al complexes. Major elements were quantified via inductively coupled plasma optical emission spectrometry (ICP-OES) and trace metals via inductively coupled plasma mass spectrometry (ICP-MS). All data were within 10% of certified values (relative to international reference material SBC-1), except for Mo, which was within 11%, and RSDs were within 5% for all elements.

Framework for redox and weathering interpretations

The Fe speciation proxy uses the ratio Fe_{HR}/Fe_{T} to evaluate the redox state of the water column, where values below 0.22 are considered oxic, and Fe_{HR}/Fe_{T} ratios >0.38 indicate anoxic conditions, with elevated ratios arising as a result of the additional water column precipitation of Fe_{HR} phases (Raiswell and Canfield 1998; Raiswell et al. 2018). Values between these ratios are considered equivocal (Poulton and Canfield 2011; Poulton 2021). For samples deposited in anoxic waters, the ratio Fe_{py}/Fe_{HR} can be applied to differentiate between ferruginous (Fe-containing; where Fe_{py}/Fe_{HR} ratios are commonly <0.6) and euxinic (anoxic and sulfidic) conditions (where Fe_{py}/Fe_{HR} ratios are commonly >0.8), with ratios between 0.6 and 0.8 considered equivocal (Poulton 2021).

The Fe speciation proxies have been extensively calibrated in modern and ancient settings (Raiswell and Canfield 1998; Raiswell et al. 2001; Poulton and Raiswell 2002; Clarkson et al. 2014), with the latter, by definition, incorporating the effects of diagenesis (see Pasquier et al. 2022). In addition, however, we consider our Fe speciation data alongside independent RSTE (specifically U, Mo, V,

Re) systematics, to provide a particularly robust assessment of the chemical conditions of deposition (e.g. Takahashi et al. 2021; Zirks et al. 2021; He et al. 2022; Li et al. 2023). Redox-sensitive trace elements provide additional information owing to the different solubility of the metals depending on the redox state at the time of deposition, which affects RSTE enrichment levels in the sediments. Specifically, in oxic seawater, U and Mo are commonly present as dissolved U(VI) and Mo(VI) (Calvert and Pedersen 1993; Zheng et al. 2000). However, under anoxic conditions, U(VI) is reduced to insoluble U(IV) (Anderson et al. 1989), whereas in the specific presence of relatively high concentrations of dissolved sulfide, Mo (VI) forms thiomolybdates (MoO_xS₄ $^{x-}$), which are particle reactive and may be sequestered in the sediment (Helz et al. 1996; Zheng et al. 2002). Vanadium behaves in a similar redox-sensitive fashion to U, and is commonly transported to sediments as the vanadate ion (H₂V(VI)O₄) adsorbed onto Mn oxides. Under dysoxic porewater conditions, where Mn oxides are reduced to Mn²⁺, V is commonly released from sediments (Emerson and Huested 1991; Nameroff et al. 2002). However, under anoxic conditions, the vanadate released following Mn oxide reduction is reduced to the vanadyl ion $(V(IV)O^{2+})$, which is highly surface-reactive and tends to be retained in the sediment (Emerson and Huested 1991). Rhenium is particularly sensitive to weakly reducing (dysoxic) conditions and is enriched in sediments where dysoxic conditions occur in the water column or just below (c. 1 cm) the sediment–water interface (Crusius et al. 1996).

Thus, consideration of RSTE systematics alongside Fe speciation data ultimately allows oxic, dysoxic, ferruginous and euxinic conditions to be distinguished. However, redox-sensitive trace elements can also be controlled by intrinsic basinal factors, such as provenance, and to (partially) account for this (see below) we calculate enrichment factors (EF) to normalize the concentration of RSTE to average upper continental crust (UCC; McLennan 2001), where the enrichment factor for a specific element ($X_{\rm EF}$) = $(X/AI)_{\rm sample}/(X/AL)_{\rm UCC}$.

We also utilize the chemical index of alteration (CIA) weathering proxy (Nesbitt and Young 1982), which is based on the differential mobility of cations as chemical weathering intensity varies, and is calculated as

$$CIA = [Al_2O_3/(Al_2O_3 + CaO^* + Na_2O + K_2O] \times 100$$

where oxides are in molar units and CaO* represents CaO in the silicate fraction. The silicate CaO fraction was determined following a correction for Ca present as apatite. With this proxy, low values indicate relatively low weathering intensity and are thus considered to reflect more arid and polar conditions, whereas higher values suggest a warmer and wetter climate.

Results

Organic carbon isotopes and concentrations

The $\delta^{13}C_{org}$ profile is rather constant through the Lower Hartfell Shale, with values of $-32\pm0.21\%$, before an abrupt increase to c.-29% at the base of Upper Hartfell Shale (Fig. 2; all geochemical data are reported in the Supplementary material Tables S1–S3). This is followed by a slight overall increase through the *Dicellograptus complanatus* Zone and into the *Dicellograptus anceps* Zone. A gradual decline to c.-33% then occurs towards the end of the Katian, although there is considerable variability (Fig. 2). This was followed by a positive excursion in the early Hirnantian, before a rapid drop in the late Hirnantian and the return of stable low values that persist into the Silurian. Thus, both black shale units at Dob's Linn are associated with relatively low $\delta^{13}C_{org}$ values (c.-32%), whereas the intervening organic-poor mudstones of the Upper Hartfell Shale have higher values (Fig. 2). These trends are broadly comparable with those

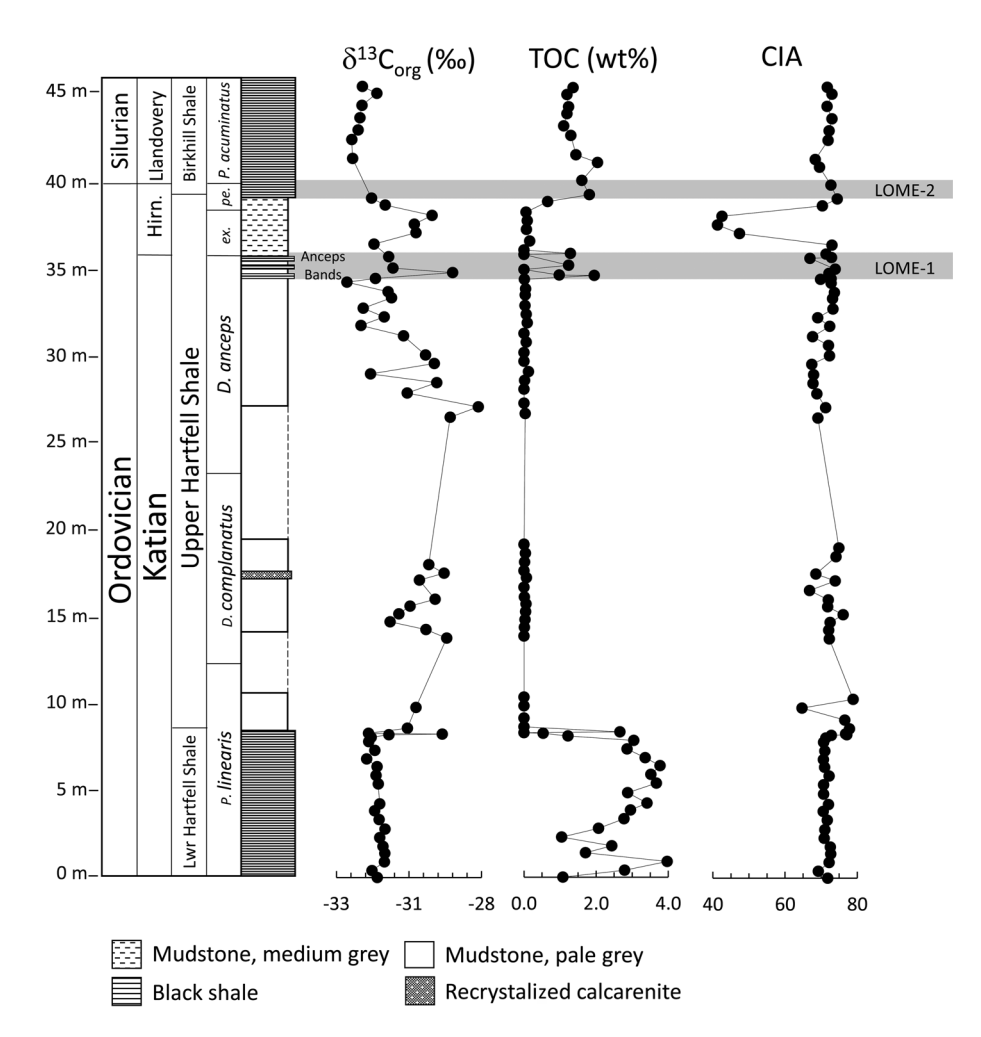


Fig. 2. Geochemical profiles for $\delta^{13}C_{org}$, TOC and CIA at Dob's Linn. *ex.* is *extraordinarius* and *pe.* is *persculptus*. The extinction levels LOME-1 and LOME-2 are based on the last occurrences of graptolites in this section (Williams 1988) and coincide with the global extinction losses of many other marine groups (e.g. Harper *et al.* 2014).

obtained in previous studies at Dob's Linn (Underwood *et al.* 1997; Bond and Grasby 2020). In detail, Underwood *et al.* (1997) recorded more stable $\delta^{13}C_{org}$ values between -32 and -31% in the latest Katian, although this may be a reflection of the low sample density, with only seven samples across 25 m of section. Bond and Grasby (2020) analysed only the uppermost 15 m of the Katian, but this included the gap in our data between 18 and 27 m height, which we found to be inaccessible (Fig. 2). They noted a minor negative excursion of c. 1‰ magnitude at this level. Our data from the topmost Ordovician and earliest Silurian broadly match the detailed record from Bond and Grasby (2020), which begins in the late Katian and shows a major negative excursion at the base of the Birkhill Shale.

The total organic carbon record shows relatively high values in the Lower Hartfell Shale, with an average of 2.58 ± 1.03 wt% (Fig. 2). These values decline substantially in the Upper Hartfell Shale, remaining low $(0.23 \pm 0.59$ wt%) throughout most of this interval. However, there is more variability towards the top of the Upper Hartfell Shale, with peaks of up to 1.95 wt% in several thin black shales (*Anceps* Bands) that occur at this level. Organic carbon values drop again above this level in the grey mudstones of the uppermost Upper Hartfell Shale $(0.17 \pm 0.24$ wt%). The onset of the black shale-dominated Birkhill Shale in the late Hirnantian sees TOC values increase again, to an average of 1.43 ± 0.30 wt%. Inorganic C concentrations are low $(0.24 \pm 0.52$ wt%) throughout most of the section (Supplementary material Table S1).

Fe speciation

Samples from the Lower Hartfell Shale have a low total iron content (Fig. 3). These values are below the threshold (0.5 wt%) generally considered to provide reliable Fe speciation data (Clarkson *et al.* 2014). However, these thresholds were developed for carbonates,

which is not the case in the current study, and fluctuations in Fe speciation data are broadly consistent with the RSTE data (see below), suggesting a robust redox signal is preserved (see also Poulton *et al.* 2015). A sharp rise in Fe_T concentrations occurs at the Lower–Upper Hartfell Shale transition, with values averaging 4.87 ± 1.17 wt% in the Upper Hartfell Shale, and values remain well above the 0.5 wt% threshold throughout the remainder of the section (Fig. 3).

The Lower Hartfell Shale and basal Upper Hartfell Shale Fe_{HR}/Fe_{T} ratios show considerable variability, with values ranging from <0.22 to >0.38 (Fig. 4). Fe_{py}/Fe_{HR} ratios mostly plot below 0.6, with the exception of four samples that plot above this value towards the top of the interval (Fig. 4). Throughout most of the remaining pale grey mudstones of the Upper Hartland Shale, Fe_{HR}/Fe_{T} ratios fluctuate between <0.22 and 0.22–0.38, and with the exception of two samples Fe_{py}/Fe_{HR} ratios are very low. However, elevated Fe_{HR}/Fe_{T} ratios (>0.38) occur just below and in the thin black shales of the *Anceps* Bands, where Fe_{py}/Fe_{HR} ratios remain below 0.6 (Fig. 4). Fe_{HR}/Fe_{T} ratios are then dominantly >0.38 (0.66 ± 0.22) in the Birkhill Shale, and Fe_{py}/Fe_{HR} ratios rise to values that are close to, or above, 0.6 (Fig. 4).

Redox-sensitive trace elements

Overall, RSTE concentrations are relatively high in the Lower Hartland Shale (Fig. 3), although the individual elements show different degrees of variability (Mo = 8.4 ± 4.5 ppm; U = 8.9 ± 2.9 ppm; V = 483.6 ± 189.4 ppm; Re = 36.7 ± 22.6 ppb). Trace metal concentrations are persistently low throughout most of the Upper Hartfell Shale (Mo = 1.8 ± 3.1 ppm; U = 3.4 ± 3.6 ppm; V = 123.7 ± 34.2 ppm; Re = 8.7 ± 9.6 ppb). However, peaks in RSTE concentrations occur in the interval with the thin black shales of the *Anceps* Bands. Low trace metal concentrations then persist through the lower part of the Hirnantian, but U and Re (and possibly Mo)

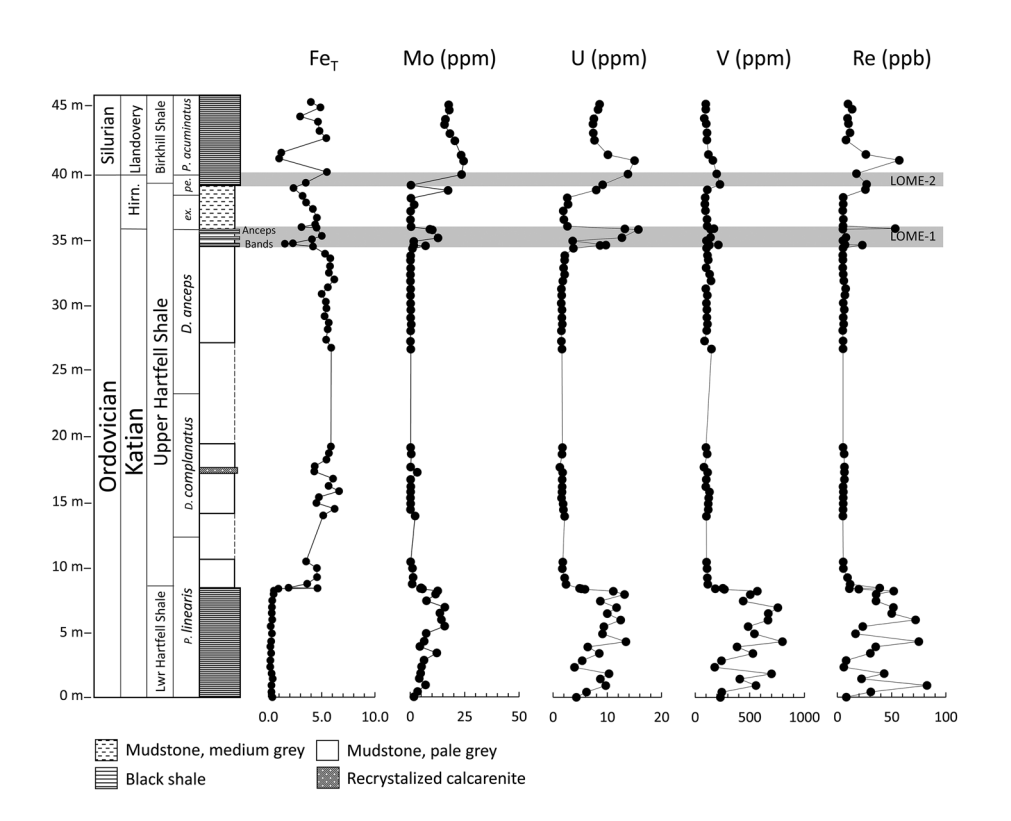


Fig. 3. Geochemical profiles for total Fe (Fe_T) and trace metals (Mo, U, V and Re) at Dob's Linn.

begin to increase in the latter half of the Hirnantian, followed by a slightly delayed increase in V (Fig. 3). These results are similar to the data obtained by Bond and Grasby (2020) for Mo and U, which show an increase across the Ordovician–Silurian boundary. Coincident with an overall increase in Fe $_{\rm HR}/{\rm Fe}_{\rm T}$ ratios (Fig. 4), RSTE concentrations continue to increase (with some fluctuations) with the onset of black shale deposition at the base of the Birkhill Shale (Fig. 3). All of the RSTE profiles then show an overall decrease through the Birkhill Shale, although Mo and U concentrations remain relatively high (Fig. 3).

Chemical index of alteration

The CIA profile shows consistently high values (70.61 ± 6.19), with a very limited degree of variability, throughout most of the section

(Fig. 2). The exception occurs during the mid-Hirnantian, where values decrease dramatically, reaching a nadir of *c*. 43 around the *extraordinarius–persculptus* boundary, before increasing to background values at the onset of the Birkhill Shale.

Discussion

Sediment source and palaeoclimate

Aluminium concentrations are low $(3.88 \pm 1.89 \text{ wt}\%)$ in the Lower Hartfell Shale (average UCC = 8.04 wt%), as are the other major elements measured in this study (see Supplementary material Table S1). Because the chemical composition of the Lower Hartfell Shale is not appreciably diluted by very high concentrations of TOC $(2.80 \pm 0.98 \text{ wt}\%; \text{Fig. 2})$ or TIC $(0.18 \pm 0.32 \text{ wt}\%; \text{Supplementary})$

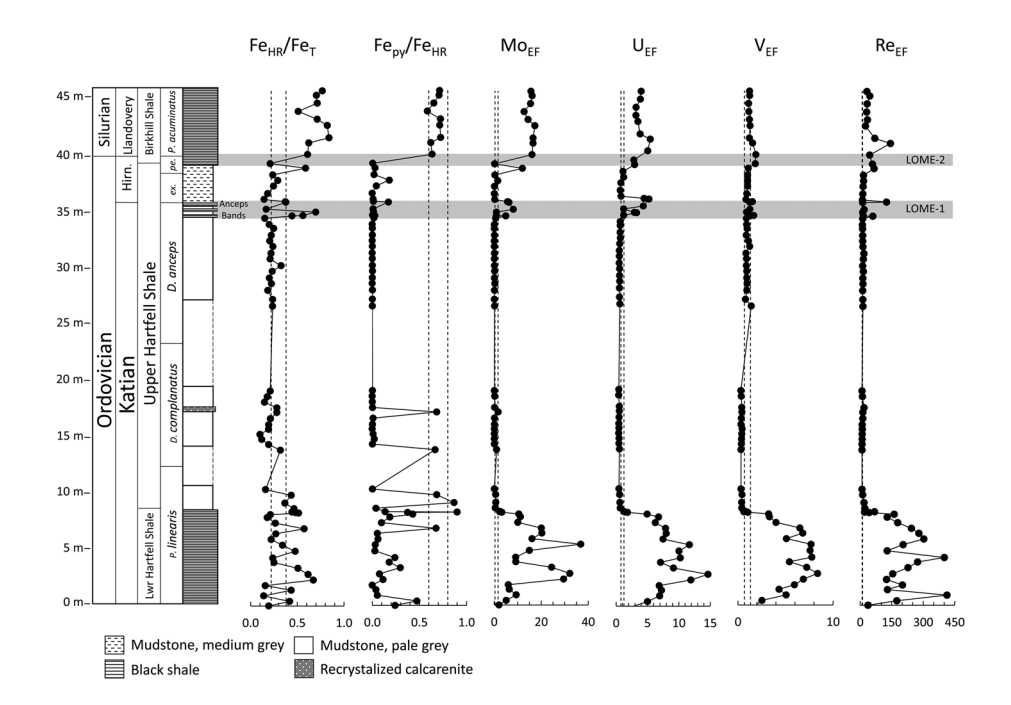


Fig. 4. Geochemical profiles for Fe_{HR}/Fe_{T} , Fe_{py}/Fe_{HR} and trace metal enrichment factors. The lines on the Fe_{HR}/Fe_{T} plot represent the boundary for distinguishing oxic and anoxic water column conditions. The lines on the Fe_{py}/Fe_{HR} plots represent the boundaries for distinguishing euxinic (>0.8) and ferruginous (<0.6) water column conditions. The dashed lines in the enrichment factor plots represent the average oxic baseline ranges (average \pm 1SD).

material Table S1), a relatively high siliceous content is implied (note that silica cannot be directly determined via the dissolution technique we employed). A high silica content is typical of oceanic sediments that are far removed from terrigenous runoff, where wind-blown silica can be important, along with biogenic silica derived from radiolarians (Cecil 2015; Kidder and Tomescu 2016), although no radiolarians are seen in the case of the Dob's Linn sediments (Armstrong and Coe 1997). Aluminium concentrations are higher in the sediments overlying the Lower Hartfell Shale (8.95 \pm 1.69 wt%), but a deep oceanic setting is still supported by the very low sedimentation rates noted above, which are characteristic of abyssal plains. The prolonged stability of the CIA values at Dob's Linn (Fig. 2) further suggests that this was a distal location in which local changes in sediment provenance were averaged out.

The only climatic event to register in the Dob's Linn strata is the Hirnantian glaciation, recorded by a dramatic decline in CIA values in the three highest grey mudstone samples from the Upper Hartfell Shale, which belong to the late extraordinarius and basal pacificus zones (Fig. 2). Similar declines in CIA values have been reported in the mid-Hirnantian of other regions, which are interpreted to reflect a decrease in weathering intensity during extensive climatic cooling (Finnegan et al. 2011; Zou et al. 2018b; Li et al. 2021). Major climatic changes have also been suggested to occur within the Katian (Young et al. 2023), including a potential warming episode in the Late Katian known as the Boda Event, which was associated with enhanced carbonate deposition (Fortey and Cocks 2005). However, our CIA results show no appreciable change during this period, meaning that, at best, it was probably a very weak event. Instead, our results are consistent with those of Barney and Grossman (2022), who suggested warm temperatures throughout the Katian, as shown by the consistent high values throughout the whole period (Fig. 2).

Ocean redox changes

Lower Hartfell Shale

Like Southern Upland strata generally, the sediments at Dob's Linn have a high thermal maturity, as indicated by high reflectance values for organic chitinozoans (in the range 3.6-4.8% R₀; Pearce et al. 1991), indicating substantial loss of TOC during burial. Despite this, considerable TOC is preserved in the Lower Hartfell Shale $(2.80 \pm 0.98 \text{ wt}\%)$ relative to most of the overlying Upper Hartfell Shale (Fig. 2), suggestive of enhanced preservation under dominantly low oxygen conditions. However, a combined evaluation of Fe speciation and RSTE systematics provides more detailed insight into the redox state of the water column. The RSTE enrichment factor profiles show a distinct overall increase through the lower part of the Lower Hartfell Shale (but with considerable fluctuation), followed by a subsequent overall decrease, whereas FeHR/FeT ratios suggest fluctuations between oxic or dysoxic (Fe $_{HR}$ /Fe $_{T}$ < 0.22) and anoxic (Fe_{HR}/Fe_T>0.38) water column conditions (Fig. 4). In addition, minima in V_{EF} values tend to coincide with peaks in Re_{EF} values, both of which are consistent with the periodic development of dysoxic conditions close to the sediment-water interface, rather than fully anoxic conditions (see Emerson and Huested 1991; Crusius et al. 1996; Nameroff et al. 2002). Furthermore, although there are slight offsets, peaks in Mo_{EF} , U_{EF} and V_{EF} (all of which are consistent with anoxic bottom water conditions) tend to coincide with peaks in FeHR/FeT ratios that are similarly indicative of anoxic conditions (Fig. 4). Taken together, these observations suggest a dynamic water column, where the redox state of bottom waters varied between dysoxic and fully anoxic.

Through the Lower Hartfell Shale interval, Fe_{py}/Fe_{HR} ratios are dominantly below 0.6 (Fig. 4), suggesting that when the water column was anoxic, it was ferruginous rather than euxinic

(Poulton and Canfield 2011; Poulton 2021). This interpretation can be further evaluated by co-consideration of Mo_{EF} and U_{EF} systematics, whereby a cross-plot of these parameters (Fig. 5) can provide detailed insight into the redox chemistry of the water column and the mechanism of Mo enrichment in the sediment (Algeo and Tribovillard 2009; Tribovillard et al. 2012). A complication when constructing such plots is that the chemical composition of the sediment supplied to the local region may differ considerably from the UCC composition used to calculate enrichment factors (e.g. Algeo and Li 2020; Bennett and Canfield 2020; Li et al. 2023). Ideally, for these plots to be valid, U and Mo enrichment factors should be close to unity for sediments deposited under oxic conditions. However, particularly for the middle portion of the Upper Hartfell Shale, U and Mo enrichment factors calculated relative to UCC are very low (U = 0.55 ± 0.15 ; $Mo = 0.27 \pm 0.36$). All of the independent redox proxies indicate that this portion of the section was deposited under oxic conditions (see discussion below), and because there is no evidence for a change in sediment provenance (see above), this allows us to define average oxic baseline averages for the Dob's Linn strata. Using these averages, we thus scale our U and Mo enrichment factor data, such that the average value for the Upper Hartfell Shale oxic samples is unity.

This exercise shows that the majority of Lower Hartfell Shale samples plot between the dysoxic and anoxic non-sulfidic fields (Fig. 5). The RTSE data thus provide strong support for deposition under redox conditions that dominantly fluctuated between dysoxic and anoxic ferruginous (Algeo and Tribovillard 2009; Tribovillard *et al.* 2012). It is possible that the two Lower Hartfell Shale samples with elevated Fe_{py}/Fe_{HR} ratios (Fig. 4) were deposited during brief euxinic episodes. However, by analogy with the two samples at the base of the Upper Hartfell Shale that also have elevated Fe_{py}/Fe_{HR} ratios but lack Mo enrichment (Fig. 4), it is perhaps more likely that the elevated degree of pyritization in these samples reflects particularly intense diagenetic pyrite formation under ferruginous water column conditions, rather than water column euxinia (Poulton 2021).

Upper Hartfell Shale

There is a marked reduction in TOC concentrations above the basal portion of the Upper Hartfell Shale (Fig. 2). This change coincides with a decline in RSTE concentrations and enrichment factors, as well as Fe_{HR}/Fe_T ratios (Figs 3 and 4), all of which strongly support a transition to persistently oxic water column conditions. In particular, the lack of any Re enrichment suggests that even the

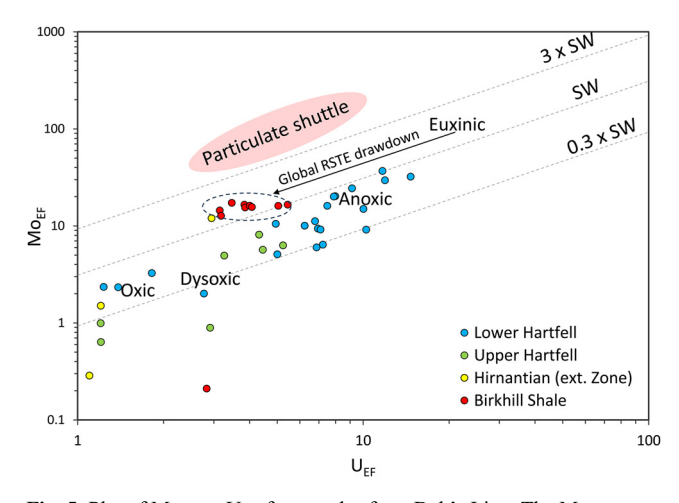


Fig. 5. Plot of Mo_{EF} v. U_{EF} for samples from Dob's Linn. The Mo_{EF} and U_{EF} values are normalized to the average oxic baseline value for Dob's Linn. Dashed lines show the proportions of the seawater (SW) Mo/U ratio.

sediment porewaters were well oxygenated close to the sedimentwater interface (Crusius et al. 1996). These conditions persisted until the latest Katian, just prior to where black shale beds a few centimetres thick (Anceps Bands) occur interbedded with medium grey mudstones typical of the remainder of the Upper Hartfell Shale. These samples are enriched in TOC (Fig. 2) and have elevated Fe_{HR}/ Fe_T ratios, as well as moderately elevated U_{EF} and Mo_{EF} values, and slightly elevated V_{EF} and Re_{EF} values (Fig. 4). These observations suggest anoxic depositional conditions for the black shales fluctuating to oxic conditions during deposition of the interbedded grey shales. The relatively low RSTE enrichments (particularly V and Re) probably reflect enhanced re-mobilization of these elements during the better-oxygenated intervals. This would have allowed oxygen to diffuse into the porewaters close to the sediment-water interface, driving V re-mobilization as porewaters became dysoxic, and additional V and Re (and probably U and Mo) re-mobilization as porewaters became fully oxic. The low Fe_{py}/Fe_{HR} ratios (Fig. 4) suggest ferruginous water column conditions for the anoxic samples in this interval, which is supported by Mo_{EF} and U_{EF} values that plot between the dysoxic and anoxic non-sulfidic fields (Fig. 5), despite the potential for U and Mo re-mobilization. However, because pyrite would also have been oxidized as porewaters became better oxygenated during the relatively short-lived oxic intervals, it is difficult to rule out intervals of euxinic depositional conditions.

In the uppermost Hartfell Shale portion of the Hirnantian, where grey mudstone occurs, TOC concentrations are low (Fig. 2), and RSTE and Fe speciation systematics (Fig. 4) initially suggest oxic depositional conditions. However, the progressive increase in TOC, RSTE enrichment factors and Fe_{HR}/Fe_{T} ratios towards the top of this interval may reflect a gradual return of anoxic conditions and enhanced organic matter preservation just prior to deposition of the Birkhill Shale.

Birkhill Shale

Elevated Fe_{HR}/Fe_T ratios and increased RSTE enrichment factors (Fig. 4), as well as higher TOC concentrations (Fig. 2), support a return to anoxic conditions at the end of the Hirnantian (although one sample towards the base has a low Fe_{HR}/Fe_T ratio coincident with a low Mo_{EF} value; Fig. 4), which persisted into the early Silurian. Euxinia is supported by persistently elevated Fe_{py}/Fe_{HR} ratios (close to or above the 0.6 threshold). However, RSTE concentrations are not particularly high (see Scott and Lyons 2012; Bennett and Canfield 2020), and V_{EF} and Re_{EF} values are particularly muted (Fig. 4). There have, however, been numerous reports of widespread anoxia and euxinia at this time, from a variety of global localities (Hammarlund et al. 2012; Zou et al. 2018b; Bond and Grasby 2020; Stockey et al. 2020). Hence, the relatively low RSTE element enrichments probably reflect global drawdown of the RSTE water column inventory owing to widespread anoxia or euxinia, as has been suggested for other intervals of widespread anoxia during the Phanerozoic (e.g. Algeo 2004; Goldberg et al. 2016). This would shift the position of the euxinic field on a U_{EF} Mo_{EF} crossplot, as shown in Figure 5.

Biotic crises and ocean redox

The second phase of the Late Ordovican mass extinction (LOME-2) has long been linked with the global spread of anoxia (e.g. Hallam and Wignall 1997; Hammarlund *et al.* 2012; Melchin *et al.* 2013; Zhou *et al.* 2015; Zou *et al.* 2018b), which is clearly manifest in the development of ferruginous conditions at Dob's Linn (Figs 3 and 4). By contrast, the LOME-1 interval has been linked with the onset of the Hirnantian glaciation, and many early studies suggested that this mass extinction phase was caused by intense cooling (Stanley 1988; Hallam and Wignall 1997; Melchin *et al.* 2013). However, recent

studies have instead highlighted evidence for marine anoxia around the Katian–Hirnantian boundary and have linked LOME-1 with widespread anoxia (Harper *et al.* 2014; Zou *et al.* 2018*b*; Dahl *et al.* 2021; Li *et al.* 2021). In some areas, euxinic conditions appear to have been prevalent (e.g. Zou *et al.* 2018*b*), but in other areas the redox conditions may have been mostly ferruginous (e.g. Hammarlund *et al.* 2012), which is supported by a negative shift in the oceanic sulfate record (recorded by carbonate-associated sulfate, $\delta^{34}S_{CAS}$, values), potentially indicating that pyrite burial fluxes decreased at this time (Kozik *et al.* 2022).

The timing of the first phase of extinction at Dob's Linn supports a link with the development of anoxic ferruginous conditions. The graptolite record shows a major loss of graptolites in the latest Katian Paraorthrograptus pacificus Zone (Williams 1988). The disappearances occur within the Anceps Bands, with only 13 species surviving into the highest band, and only two surviving above this in the Hirnantian (Williams 1988; Mitchell and Melchin 2020). These losses clearly occur before the CIA evidence of glaciation at Dob's Linn (Fig. 2). Studies of the end Katian anoxic event in South China show that it can be resolved as an interval of fluctuating, variable redox conditions rather than the more stable and intense anoxia developed at the Ordovician-Silurian boundary (Zou et al. 2018b; Yan et al. 2019). This is matched by the Iapetus Ocean record at Dob's Linn, which shows alternations from the ferruginous anoxic conditions of the Anceps Bands, to oxic conditions in the interbedded mudstones. Based on average sedimentation rates for this interval of the Dob's Linn section (see above), these alternations occurred every few tens of thousands of years. These observations support the suggestion that it was rapid fluctuations in marine oxygen levels, rather than persistent euxinia, which caused LOME-1 (Kozik et al. 2022).

Redox changes appear closely linked to both phases of the LOME, but it is difficult to evaluate causes of the earlier mid-Katian crisis because it is unclear precisely when it occurred and how long it lasted. Our study shows that there was a major redox change in the Iapetus Ocean in the late *Pleurograptus linearis* Zone, from fluctuating dysoxic to ferruginous conditions, to stable welloxygenated conditions (Fig. 4). The oxygen-depleted conditions may correspond to a major diversity decline in South China (Deng et al. 2021). However, global estimates of diversity changes using the Paleobiology Database have suggested that there was a prolonged diversity decline in the Late Katian (Rasmussen et al. 2019), but this observation is at a low temporal resolution. The improved deep ocean ventilation observed in the Dob's Linn record seems an unlikely cause of this diversity crisis, but other proposed mechanisms are also unconvincing. The controversial latest Katian warming episode, known as the Boda Event, has been invoked but it post-dated the crisis and was, in any case, associated with the flourishing of carbonate platform benthos (Rasmussen et al. 2019). Alternatively, Rasmussen et al. (2019) suggest prolonged volcanism throughout the Late Katian as a cause of the crisis. The possible culprit may be a former flood basalt province now preserved as a series of dissected remnants in northern Iran (Derakhshi et al. 2022). Eruptions in the region spanned the Katian to Early Silurian, with voluminous emissions beginning around the Sandbian-Katian boundary and climaxing around the Katian-Hirnantian boundary (Derakhshi et al. 2022). However, neither of these peak intervals appears to be a good fit with the mid-Katian crisis, as the former coincides with a phase of diversity increase (Deng et al. 2021) whereas the latter coincides with LOME-1.

There is clearly much that remains to be understood about the mid-Katian crisis, including its timing and duration, together with a need for improved understanding of environmental changes during the interval. For the time being we note that there was a major and rapid change in Iapteus Ocean ventilation in the late *P. linearis* Zone that may have been of relevance to the Katian crisis.

Ocean redox, carbon isotope fluctuations and the Hirnantian glaciation

The Hirnantian glaciation is associated with well-ventilated conditions at Dob's Linn (Fig. 4), whereas similar redox proxy data for other sections around the world suggest transitions to either oxic or dysoxic conditions (e.g. Zhou et al. 2012; Ahm et al. 2017; Smolarek et al. 2017; Bond and Grasby 2020). In South China, however, widespread euxinic conditions on the shelf appear to have been replaced by ferruginous conditions during the Hirnantian (e.g. Zou et al. 2018b; Qiu et al. 2022). Nevertheless, a common feature of these studies is a shift towards less reducing conditions (Qiu et al. 2022). By contrast, an alternative interpretation has been suggested based on pyrite sulfur isotopes from a shallow-water site on the Yangtze Platform, South China, which shows a c. 10% shift to heavier values during the Hirnantian glaciation (Zhang et al. 2009). This trend has been interpreted to reflect enhanced pyrite burial in anoxic deep waters at a time of inferred limited sulfate input to the oceans, leaving residual sulfate values in shallow waters enriched in ³⁴S, which was subsequently recorded in pyrite (Zhang et al. 2009). However, although this trend is seen on a global scale, it has alternatively been interpreted to reflect extensive drawdown of seawater sulfate under widespread euxinic conditions prior to the Hirnantian glaciation, potentially coupled with a decrease in the supply rate of sulfate from continental weathering owing to lower glacial chemical weathering rates during the Hirnantian itself (Qiu et al. 2022). This latter interpretation is supported by analyses of δ^{34} S_{CAS}, which show a large negative excursion (c. 15% amplitude) during the Hirnantian glaciation, suggesting that there was a major decline in pyrite formation (Kozik et al. 2022) that allowed the seawater sulfate reservoir to gradually replenish through the glaciation, despite relatively low chemical weathering rates (Qiu

Carbon isotope fluctuations provide additional insight into global-scale changes. In the Katian, δ^{13} C values show substantial fluctuations (Fig. 2), with distinct regional variations, but no overall correlatable trends between sections (Cramer and Jarvis 2020). By contrast, the early Hirnantian is marked by a major positive excursion of c. 6% magnitude in carbonates, which has been identified in numerous sections globally (e.g. Fan et al. 2009; Cramer and Jarvis 2020). The excursion, known as the Hirnantian Isotopic Carbon Excursion (HICE), is seen at Dob's Linn in our data (Fig. 2), and is generally interpreted to record enhanced burial of isotopically light organic matter during an oceanic anoxic event (e.g. Saltzman and Young 2005; Young et al. 2010; Hammarlund et al. 2012; Harper et al. 2014; Yan et al. 2019). However, the excursion occurs during the Hirnantian glaciation, an interval associated with a global decrease in organic-rich shale deposition in shelf sections (Qiu et al. 2022). To avoid this 'problem', enhanced organic carbon accumulation is commonly considered to have occurred in deeper ocean settings (e.g. Zhang et al. 2009; Hammarlund et al. 2012; Pohl et al. 2021). Using the cGENIE Earth system model, Pohl et al. (2021) provided a scenario for the Hirnantian glaciation in which surface waters became better oxygenated whereas deep oceans became anoxic. Thus, deepwater formation during the late Katian warm interval is envisaged to have occurred at high northern latitudes in the northern Panthalassic Ocean, ensuring that strong meridional overturn ventilated deep oceans over much of the world (Pohl et al. 2021). Subsequently, the formation of sea ice at polar latitudes during Hirnantian cooling led to a shutdown of deep-water formation, causing a decline in deepwater oxygenation. However, these cGENIE model results are not supported by our deep ocean record from Dob's Linn, which shows that the Iapetus Ocean was well ventilated during the Hirnantian glaciation, at a time when less reducing conditions also developed on the shelf.

The evidence from Dob's Linn indicates that the HICE was unlikely to have been caused by enhanced organic C burial, and its origin therefore requires an alternative scenario. Melchin and Holmden (2006) ascribed the HICE to weathering of carbonate successions during the glacial lowstand, although the ability of this process to cause such a major excursion has been questioned (Fan et al. 2009). Nonetheless, the HICE could be recording a change in carbonate burial fluxes. Biogeochemical modelling of a major positive carbon isotope excursion during the Middle Permian, called the Kamura event, has suggested that a combination of a decline in chemical weathering rates and an associated reduction in carbonate burial best explains the positive carbon isotope trend at this time (Zhang et al. 2020). The decline in chemical weathering during the Kamura Event has been attributed to aridification of Pangaea in the Middle Permian (Zhang et al. 2020), but the same effect could also have been achieved in the Hirnantian by cooling during glaciation, as seen in the CIA record (Fig. 2). We therefore suggest that the HICE may record a major decline in carbonate production, and not an increase in organic C burial or carbonate weathering.

A role for volcanism?

Many extinction crises coincide with vast outpourings of flood basalts, with the result that most extinction models invoke volcanism in their kill mechanisms (e.g. Bond and Wignall 2014; Wignall 2015; Gong et al. 2017). However, the end-Ordovician crisis has long remained an outlier to this pattern, with no known associated flood basalt province. Late Ordovician-Early Silurian basalts in northern Iran are possibly the remnants of such a province (Derakhshi et al. 2022), but the available age dating suggests that most of the volcanism in this region substantially predates the LOME. Lacking direct evidence for volcanism, mercury enrichment in sedimentary successions has widely been used to infer major volcanic episodes. Thus, several recent studies have noted Hg spikes in latest Ordovician strata (Gong et al. 2017; Jones et al. 2017; Smolarek-Lach et al. 2019), including, most recently, at Dob's Linn (Bond and Grasby 2020). However, there is little consistency in the levels of enrichment between regions, with Hg/TOC spikes ranging from the mid-Katian to the Early Silurian, and with the highest values occurring above the LOME-2 horizon.

Clearly, there was substantial volcanism over a prolonged interval. However, an especially large but brief Hg/TOC spike is evident at the Katian-Hirnantian boundary in the records of Jones et al. (2017) and Smolarek-Lach et al. (2019), indicating that volcanism was especially intense at the onset of LOME-1. Speculation that this volcanism caused or intensified glaciation at this time (Jones et al. 2017) is not supported by our CIA data, nor palaeotemperature estimates, which show there was minor transient warming at this stage boundary (Finnegan et al. 2011). Other volcanism-extinction links generally favour global warming scenarios, triggered by the release of volcanic CO₂, and consequent changes in oceanic circulation and redox (Bond and Grasby 2020). Nonetheless, the role of volcanism in the LOME events currently remains speculative, owing to the lack of a known volcanic centre and the rather sporadic Hg spike record from this interval. Moreover, Shen et al. (2022) suggested that Hg spikes may be caused by elevated drawdown of Hg under euxinic conditions, rather than being due to enhanced volcanism.

Conclusions

The cause of the late Ordovician mass extinction is debated, with diverse environmental changes, including a short intense glaciation and major oceanic redox fluctuations, providing possible drivers. Here, we interpret the Dob's Linn stratotype (southern Scotland) to record conditions in the distal Iapetus Ocean, thus providing a

valuable record of open-ocean conditions. A multi-proxy assessment of redox conditions, using iron speciation and RSTE data, reveals dysoxic to anoxic ferruginous conditions in the mid-Katian, followed by a major improvement in Iapetus oxygenation in the late Katian. This was followed by rapid redox fluctuations from anoxic ferruginous to oxic conditions at the end of the Katian, an interval that coincides with the first phase of the end-Ordovician mass extinction that was marked by substantial graptolite species losses at Dob's Linn. Thus, redox fluctuations may have been the main stressor for the pelagic graptolites. This was followed by improved oxygenation in the Hirnantian and a major, short-lived decline in the chemical index of alteration, which suggests decreased chemical weathering in the distal hinterland as a consequence of glaciation. The timing of this intense cooling clearly postdates the end-Katian graptolite extinctions, thus weakening purported links between the Hirnantian glaciation and the Late Ordovician mass extinction.

Explanations for the positive carbon isotope excursion during the Hirnantian glaciation have generally relied on increased organic matter burial in deep ocean settings, but the Dob's Linn sediments do not support this scenario. Alternatively, the positive excursion could reflect a drastic decline in carbonate burial in the cool climate of the Hirnantian. Post-glaciation, the Iapetus Ocean once again became poorly ventilated in the latest Hirnantian, at a time marked by a second phase of extinctions. Anoxia, and in particular, euxinia, persisted into the Silurian, a time of widespread black shale deposition, and the relatively muted trace metal enrichments observed during this interval at Dob's Linn probably reflect intense drawdown of redox-sensitive trace elements from the oceans.

Recent studies have identified a mid-Katian biotic crisis prior to the Late Ordovician mass extinction, although the precise level of the losses has yet to be clarified, and causative mechanisms are unclear. The mid-Katian record at Dob's Linn records a major and prolonged oceanic oxygenation event, where dysoxic to anoxic ferruginous conditions were replaced by well-oxygenated conditions. This clear change in oceanic redox suggests a major reorganization of oceanic circulation but its detailed links with the biotic crisis remain to be investigated.

Scientific editing by Laishi Zhao

Acknowledgements We are grateful to two anonymous reviewers for helpful comments, and to Laishi Zhao and Y. Dilek for editorial handling.

Author contributions As-R: data curation (lead), formal analysis (equal), investigation (equal), methodology (equal), visualization (equal), writing – original draft (lead), writing – review & editing (supporting); PBW: conceptualization (equal), formal analysis (equal), investigation (equal), methodology (equal), project administration (equal), resources (equal), supervision (equal), validation (equal), visualization (equal), writing – original draft (supporting), writing – review & editing (equal), YX: methodology (equal), validation (equal); SWP: conceptualization (equal), formal analysis (equal), funding acquisition (lead), investigation (equal), methodology (equal), project administration (equal), resources (equal), supervision (equal), validation (equal), visualization (equal), writing – original draft (supporting), writing – review & editing (equal)

Funding This study was supported by funds from the School of Earth and Environment, University of Leeds, and by NERC grant NE/T008458/1 (S.W.P.).

Competing interests The authors declare that they have no known competing financial interests or personal relationships that could have appeared to influence the work reported in this paper.

Data availability All data generated or analysed during this study are included in this published article and its supplementary information files.

References

- Ahm, A.-S.C., Bjerrum, C.J. and Hammarlund, E.U. 2017. Disentangling the record of diagenesis, local redox conditions, and global seawater chemistry during the latest Ordovician glaciation. *Earth and Planetary Science Letters*, **459**, 145–156, https://doi.org/10.1016/j.epsl.2016.09.049
- Alcott, L.J., Krause, A.J. et al. 2020. Development of iron speciation reference materials for palaeoredox analysis. *Geostandards and Geoanalytical Research*, 44, 581–591, https://doi.org/10.1111/ggr.12342
- Algeo, T.J. 2004. Can marine anoxic events draw down the trace element inventory of seawater? *Geology*, 32, 1057, https://doi.org/10.1130/G20896.1
- Algeo, T.J. and Li, C. 2020. Redox classification and calibration of redox thresholds in sedimentary systems. *Geochimica et Cosmochimica Acta*, 287, 8–26, https://doi.org/10.1016/j.gca.2020.01.055
- Algeo, T.J. and Tribovillard, N. 2009. Environmental analysis of paleoceanographic systems based on molybdenum-uranium covariation. *Chemical Geology*, 268, 211–225, https://doi.org/10.1016/j.chemgeo.2009.09.001
- Anderson, R.F., Fleisher, M.Q. and LeHuray, A.P. 1989. Concentration, oxidation state, and particulate flux of uranium in the Black Sea. Geochimica et Cosmochimica Acta, 53, 2215–2224, https://doi.org/10.1016/0016-7037(89)90345-1
- Armstrong, H.A. and Coe, A.L. 1997. Deep-sea sediments record the geophysiology of the late Ordovician glaciation. *Journal of the Geological Society, London*, **154**, 929–934, https://doi.org/10.1144/gsjgs. 154.6.0929
- Armstrong, H.A. and Harper, D.A.T. 2014. An earth system approach to understanding the end-Ordovician (Hirnantian) mass extinction. *In*: Keller, G. and Kerr, A.C. (eds) *Volcanism, Impacts, and Mass Extinctions: Causes and Effects*. Geological Society of America, 287–300, https://doi.org/10.1130/2014.2505(14)
- Barney, B.B. and Grossman, E.L. 2022. Reassessment of ocean paleotemperatures during the Late Ordovician. *Geology*, 50, 572–576, https://doi.org/10.1130/G49422.1
- Bennett, W.W. and Canfield, D.E. 2020. Redox-sensitive trace metals as paleoredox proxies: a review and analysis of data from modern sediments. *Earth-Science Reviews*, **204**, https://doi.org/10.1016/j.earscirev.2020.103175
- Berry, W.B.N. and Wilde, P. 1978. Progressive ventilation of the oceans; an explanation for the distribution of the lower Paleozoic black shales. *American Journal of Science*, **278**, 257–275, https://doi.org/10.2475/ajs.278.3.257
- Bond, D.P.G. and Grasby, S.E. 2020. Late Ordovician mass extinction caused by volcanism, warming, and anoxia, not cooling and glaciation. *Geology*, 48, 777–781, https://doi.org/10.1130/G47377.1
- Bond, D.P.G. and Wignall, P.B. 2014. Large igneous provinces and mass extinctions: an update. *Geological Society of America, Special Papers*, 505, 29–55, https://doi.org/10.1130/2014.2505(02)
- Brenchley, P.J. and Štorch, P. 1989. Environmental changes in the Hirnantian (upper Ordovician) of the Prague Basin, Czechoslovakia. *Geological Journal*, **24**, 165–181, https://doi.org/10.1002/gj.3350240302
- Brenchley, P.J., Marshall, J.D. *et al.* 1994. Bathymetric and isotopic evidence for a short-lived Late Ordovician glaciation in a greenhouse period. *Geology*, **22**, 295–298, https://doi.org/10.1130/0091-7613(1994)022<0295:BAIEFA>2.3. CO:2
- Brenchley, P.J., Marshall, J.D. and Underwood, C.J. 2001. Do all mass extinctions represent an ecological crisis? Evidence from the Late Ordovician. *Geological Journal*, **36**, 329–340, https://doi.org/10.1002/gj.880
- Calvert, S.E. and Pedersen, T.F. 1993. Geochemistry of recent oxic and anoxic marine sediments: implications for the geological record. *Marine Geology*, 113, 67–88, https://doi.org/10.1016/0025-3227(93)90150-T
- Canfield, D.E., Raiswell, R., Westrich, J.T., Reaves, C.M. and Berner, R.A. 1986. The use of chromium reduction in the analysis of reduced inorganic sulfur in sediments and shales. *Chemical Geology*, **54**, 149–155, https://doi.org/10.1016/0009-2541(86)90078-1
- Cecil, C.B. 2015. Paleoclimate and the Origin of Paleozoic Chert: time to reexamine the origins of chert in the rock record. *Sedimentary Record*, 13, 4–10, https://doi.org/10.2110/sedred.2015.3.4
- Clarkson, M.O., Poulton, S.W., Guilbaud, R. and Wood, R.A. 2014. Assessing the utility of Fe/Al and Fe-speciation to record water column redox conditions in carbonate-rich sediments. *Chemical Geology*, 382, 111–122, https://doi. org/10.1016/j.chemgeo.2014.05.031
- Cocks, L.R.M. and Torsvik, T.H. 2021. Ordovician palaeogeography and climate change. Gondwana Research, 100, 53–72, https://doi.org/10.1016/j.gr.2020. 09 008
- Cramer, B.D. and Jarvis, I. 2020. Carbon isotope stratigraphy. *In*: Gradstein, F., Ogg, J.G., Schmitz, M.D. and Ogg, G.M. (eds) *Geologic Time Scale 2020*. Elsevier, Amsterdam, 309–343, https://doi.org/10.1016/B978-0-12-824360-2.00011-5
- Crusius, J., Calvert, S., Pedersen, T. and Sage, D. 1996. Rhenium and molybdenum enrichments in sediments as indicators of oxic, suboxic and sulfidic conditions of deposition. *Earth and Planetary Science Letters*, **145**, 65–78, https://doi.org/10.1016/S0012-821X(96)00204-X
- Dahl, T.W., Hammarlund, E.U., Rasmussen, C.M.Ø., Bond, D.P.G. and Canfield, D.E. 2021. Sulfidic anoxia in the oceans during the Late Ordovician mass extinctions insights from molybdenum and uranium isotopic global redox proxies. *Earth-Science Reviews*, **220**, https://doi.org/10.1016/j.earscirev.2021.103748

- Deng, Y., Fan, J. et al. 2021. Timing and patterns of the Great Ordovician Biodiversification Event and Late Ordovician mass extinction: perspectives from South China. Earth-Science Reviews, 220, https://doi.org/10.1016/j.earscirev.2021.103743
- Derakhshi, M., Ernst, R.E. and Kamo, S.L. 2022. Ordovician–Silurian volcanism in northern Iran: implications for a new large Igneous Province (LIP) and a robust candidate for the Late Ordovician mass extinction. *Gondwana Research*, **107**, 256–280, https://doi.org/10.1016/j.gr. 2022.03.009
- Emerson, S.R. and Huested, S.S. 1991. Ocean anoxia and the concentrations of molybdenum and vanadium in seawater. *Marine Chemistry*, 34, 177–196, https://doi.org/10.1016/0304-4203(91)90002-E
- Fan, J., Peng, P. and Melchin, M.J. 2009. Carbon isotopes and event stratigraphy near the Ordovician–Silurian boundary, Yichang, South China. Palaeogeography, Palaeoclimatology, Palaeoecology, 276, 160–169, https://doi.org/10.1016/j.palaeo.2009.03.007
- Fan, J.-X., Shen, S.-Z. et al. 2020. A high-resolution summary of Cambrian to Early Triassic marine invertebrate biodiversity. Science, 367, 272–277, https:// doi.org/10.1126/science.aax4953
- Finnegan, S., Bergmann, K. et al. 2011. The magnitude and duration of Late Ordovician–Early Silurian glaciation. Science, 331, 903–906, https://doi.org/ 10.1126/science.1200803
- Fortey, R.A. and Cocks, L.R.M. 2005. Late Ordovician global warming the Boda event. *Geology*, **33**, 405, https://doi.org/10.1130/G21180.1
- Goldberg, T., Poulton, S.W., Wagner, T., Kolonic, S.F. and Rehkämper, M. 2016. Molybdenum drawdown during Cretaceous Oceanic Anoxic Event 2. Earth and Planetary Science Letters, 440, 81–91, https://doi.org/10.1016/j.epsl. 2016.02.006
- Goldman, D., Sadler, P.M., Leslie, S.A., Melchin, M.J., Agterberg, F.P. and Gradstein, F.M. 2020. The Ordovician period. *In:* Gradstein, F., Ogg, J.G., Schmitz, MD. and Ogg, G.M. (eds) *Geologic Time Scale 2020*. Elsevier, Amsterdam, 631–694, https://doi.org/10.1016/B978-0-12-824360-2.00020-6
- Gong, Q., Wang, X. et al. 2017. Mercury spikes suggest volcanic driver of the Ordovician–Silurian mass extinction. Scientific Reports, 7, 5304, https://doi. org/10.1038/s41598-017-05524-5
- Hallam, A. and Wignall, P.B. 1997. Mass Extinctions and Their Aftermath. Oxford University Press.
- Hammarlund, E.U., Dahl, T.W. et al. 2012. A sulfidic driver for the end-Ordovician mass extinction. Earth and Planetary Science Letters, 331–332, 128–139, https://doi.org/10.1016/j.epsl.2012.02.024
- Harper, D.A.T., Hammarlund, E.U. and Rasmussen, C.M.Ø. 2014. End Ordovician extinctions: a coincidence of causes. *Gondwana Research*, 25, 1294–1307, https://doi.org/10.1016/j.gr.2012.12.021
- He, T., Wignall, P.B., Newton, R.J., Atkinson, J.W., Keeling, J.F.J., Xiong, Y. and Poulton, S.W. 2022. Extensive marine anoxia in the European epicontinental sea during the end-Triassic mass extinction. *Global and Planetary Change*, 210, 103771, https://doi.org/10.1016/j.gloplacha.2022.103771
- Helz, G.R., Miller, C.V., Charnock, J.M., Mosselmans, J.F.W., Pattrick, R.A.D., Garner, C.D. and Vaughan, D.J. 1996. Mechanism of molybdenum removal from the sea and its concentration in black shales: EXAFS evidence. *Geochimica et Cosmochimica Acta*, 60, 3631–3642, https://doi.org/10.1016/ 0016-7037(96)00195-0
- Jones, D.S., Martini, A.M., Fike, D.A. and Kaiho, K. 2017. A volcanic trigger for the Late Ordovician mass extinction? Mercury data from south China and Laurentia. Geology, 45, 631–634, https://doi.org/10.1130/G38940.1
- Kidder, D.L. and Tomescu, I. 2016. Biogenic chert and the Ordovician silica cycle. *Palaeogeography, Palaeoclimatology, Palaeoecology*, **458**, 29–38, https://doi.org/10.1016/j.palaeo.2015.10.013
- Kozik, N.P., Young, S.A. et al. 2022. Rapid marine oxygen variability: driver of the Late Ordovician mass extinction. Science Advances, 8, https://doi.org/10. 1126/sciadv.abn8345
- Leggett, J.K. 1978. Eustacy and pelagic regimes in the Iapetus Ocean during the Ordovician and Silurian. Earth and Planetary Science Letters, 41, 163–169, https://doi.org/10.1016/0012-821X(78)90006-7
- Li, N., Li, C. et al. 2021. Redox changes in the outer Yangtze Sea (South China) through the Himantian Glaciation and their implications for the end-Ordovician biocrisis. Earth-Science Reviews, 212, https://doi.org/10.1016/j. earscirev.2020.103443
- Li, S., Wignall, P., Xiong, Y. and Poulton, S. 2023. Calibration of redox thresholds in black shale: insight from a stratified Mississippian basin with warm saline bottom waters. *Geological Society of America Bulletin*, 136, 1266–1286, https://doi.org/10.1130/B36915.1
- Longman, J., Mills, B.J.W., Manners, H.R., Gernon, T.M. and Palmer, M.R. 2021. Late Ordovician climate change and extinctions driven by elevated volcanic nutrient supply. *Nature Geoscience*, 14, 924–929, https://doi.org/10.1038/s41561-021-00855-5
- McLennan, S.M. 2001. Relationships between the trace element composition of sedimentary rocks and upper continental crust. *Geochemistry, Geophysics, Geosystems*, 2, https://doi.org/10.1029/2000GC000109
- Melchin, M.J. and Holmden, C. 2006. Carbon isotope chemostratigraphy in Arctic Canada: sea-level forcing of carbonate platform weathering and implications for Hirnantian global correlation. *Palaeogeography*, *Palaeoclimatology*, *Palaeoecology*, **234**, 186–200, https://doi.org/10.1016/j. palaeo.2005.10.009

- Melchin, M.J., Mitchell, C.E., Holmden, C. and Štorch, P. 2013. Environmental changes in the late Ordovician–early Silurian: review and new insights from black shales and nitrogen isotopes. *Geological Society of America Bulletin*, **125**, 1635–1670, https://doi.org/10.1130/B30812.1
- 125, 1635–1670, https://doi.org/10.1130/B30812.1

 Mitchell, C.E. and Melchin, M.J. 2020. Late Ordovician mass extinction caused by volcanism, warming, and anoxia, not cooling and glaciation: Comment. *Geology*, 48, e509–e509, https://doi.org/10.1130/G47946C.1
- Nameroff, T.J., Balistrieri, L.S. and Murray, J.W. 2002. Suboxic trace metal geochemistry in the Eastern Tropical North Pacific. Geochimica et Cosmochimica Acta, 66, 1139–1158, https://doi.org/10.1016/S0016-7037 (01)00843-2
- Nesbitt, H.W. and Young, G.M. 1982. Early Proterozoic climates and plate motions inferred from major element chemistry of lutites. *Nature*, 299, 715–717, https://doi.org/10.1038/299715a0
- Pasquier, V., Fike, D.A., Révillon, S. and Halevy, I. 2022. A global reassessment of the controls on iron speciation in modern sediments and sedimentary rocks: a dominant role for diagenesis. *Geochimica et Cosmochimica Acta*, 335, 211–230, https://doi.org/10.1016/j.gca.2022.08.037
- Pearce, R.B., Clayton, T. and Kemp, A.E.S. 1991. Illitization and organic maturity in Silurian sediments from the Southern Uplands of Scotland. Clay Minerals, 26, 199–210, https://doi.org/10.1180/claymin.1991.026.2.05
- Pohl, A., Lu, Z. et al. 2021. Vertical decoupling in Late Ordovician anoxia due to reorganization of ocean circulation. *Nature Geoscience*, 14, 868–873, https:// doi.org/10.1038/s41561-021-00843-9
- Poulton, S.W. 2021. The Iron Speciation Paleoredox Proxy. In: Lyons, T., Turchyn, A. and Reinhard, C. (eds) The Iron Speciation Paleoredox Proxy, Cambridge University Press, Cambridge, 1–24 https://doi.org/10.1017/9781108847148
- Poulton, S.W. and Canfield, D.E. 2005. Development of a sequential extraction procedure for iron: implications for iron partitioning in continentally derived particulates. *Chemical Geology*, 214, 209–221, https://doi.org/10.1016/j. chemgeo.2004.09.003
- Poulton, S.W. and Canfield, D.E. 2011. Ferruginous conditions: a dominant feature of the Ocean through Earth's history. *Elements*, 7, 107–112, https://doi. org/10.2113/gselements.7.2.107
- Poulton, S.W. and Raiswell, R. 2002. The low-temperature geochemical cycle of iron: from continental fluxes to marine sediment deposition. *American Journal of Science*, 302, 774–805, https://doi.org/10.2475/ajs.302.9.774
- Poulton, S.W., Henkel, S. et al. 2015. A continental-weathering control on orbitally driven redox-nutrient cycling during Cretaceous Oceanic Anoxic Event 2. Geology, 43, 963–966, https://doi.org/10.1130/G36837.1
- Qiu, Z., Zou, C. et al. 2022. A nutrient control on expanded anoxia and global cooling during the Late Ordovician mass extinction. Communications Earth and Environment, 3, https://doi.org/10.1038/s43247-022-00412-x
- Raiswell, R. and Canfield, D.E. 1998. Sources of iron for pyrite formation in marine sediments. *American Journal of Science*, 298, 219–245, https://doi. org/10.2475/ajs.298.3.219
- Raiswell, R., Newton, R. and Wignall, P.B. 2001. An Indicator of Water-Column Anoxia: resolution of Biofacies Variations in the Kimmeridge Clay (Upper Jurassic, U.K.). *Journal of Sedimentary Research*, 71, 286–294, https://doi. org/10.1306/070300710286
- Raiswell, R., Hardisty, D.S. et al. 2018. The iron paleoredox proxies: a guide to the pitfalls, problems and proper practice. American Journal of Science, 318, 491–526, https://doi.org/10.2475/05.2018.03
- Rasmussen, C.M.Ø., Kröger, B., Nielsen, M.L. and Colmenar, J. 2019. Cascading trend of Early Paleozoic marine radiations paused by Late Ordovician extinctions. *Earth, Atmospheric and Planetary Sciences*, 116, 7207–7213, https://doi.org/10.5281/zenodo.2586976
- Saltzman, M.R. and Young, S.A. 2005. Long-lived glaciation in the Late Ordovician? Isotopic and sequence-stratigraphic evidence from western Laurentia. Geology, 33, 109, https://doi.org/10.1130/G21219.1
- Scott, C. and Lyons, T.W. 2012. Contrasting molybdenum cycling and isotopic properties in euxinic versus non-euxinic sediments and sedimentary rocks: refining the paleoproxies. *Chemical Geology*, 324–325, 19–27, https://doi.org/ 10.1016/j.chemgeo.2012.05.012
- Sheehan, P.M. 2001. The Late Ordovician mass extinction. Annual Review of Earth and Planetary sciences, 29, 331–364, https://doi.org/10.1146/annurev. earth.29.1.331
- Shen, J., Algeo, T. and Feng, Q. 2022. Mercury isotope evidence for a non-volcanic origin of Hg spikes at the Ordovician–Silurian boundary, South China. Earth and Planetary Science Letters, 594, 117705, https://doi.org/10.1016/j.epsl.2022.117705
- Smolarek, J., Marynowski, L., Trela, W., Kujawski, P. and Simoneit, B.R.T. 2017. Redox conditions and marine microbial community changes during the end-Ordovician mass extinction event. *Global and Planetary Change*, 149, 105–122, https://doi.org/10.1016/j.gloplacha.2017.01.002
- Smolarek-Lach, J., Marynowski, L., Trela, W. and Wignall, P.B. 2019. Mercury spikes indicate a volcanic trigger for the Late Ordovician mass extinction event: an example from a deep shelf of the peri-Baltic region. *Scientific Reports*, 9, 3139, https://doi.org/10.1038/s41598-019-39333-9
- Stanley, S.M. 1988. Climatic cooling and mass extinction of Paleozoic Reef Communities. *Palaios*, 3, 228, https://doi.org/10.2307/3514533
- Stockey, R.G., Cole, D.B., Planavsky, N.J., Loydell, D.K., Frýda, J. and Sperling, E.A. 2020. Persistent global marine euxinia in the early Silurian. *Nature Communications*, 11, https://doi.org/10.1038/s41467-020-15400-y

- Stone, P. 2014. The southern uplands Terrane in Scotland a notional controversy revisited. Scottish Journal of Geology, 50, 97–123, https://doi.org/ 10.1144/sig2014-001
- Strachan, R.A. 2012. Mid-Ordovician to Silurian subduction and collision: closure of the Iapetus Ocean. In: Woodcock, N. and Strachan, R. (eds) Geological History of Britain and Ireland Wiley-Blackwell, Chichester, 110–131, https://doi.org/10.1002/9781118274064.ch7
- Takahashi, S., Hori, R.S. et al. 2021. Progressive development of ocean anoxia in the end-Permian pelagic Panthalassa. Global and Planetary Change, 207, 103650, https://doi.org/10.1016/j.gloplacha.2021.103650
- Tribovillard, N., Algeo, T.J., Baudin, F. and Riboulleau, A. 2012. Analysis of marine environmental conditions based on molybdenum-uranium covariation applications to Mesozoic paleoceanography. *Chemical Geology*, 324–325, 46–58, https://doi.org/10.1016/j.chemgeo.2011.09.009
- Underwood, C.J., Crowley, S.F., Marshall, J.D. and Brenchley, P.J. 1997. High-resolution carbon isotope stratigraphy of the basal Silurian Stratotype (Dob's Linn, Scotland) and its global correlation. *Journal of the Geological Society, London*, 154, 709–718, https://doi.org/10.1144/gsjgs. 154.4.0709
- Wang, D., Liu, Y. et al. 2022. Controls on marine primary productivity variation and organic matter accumulation during the Late Ordovician–Early Silurian transition. Marine and Petroleum Geology, 142, 105742, https://doi.org/10. 1016/j.marpetgeo.2022.105742
- Wang, G., Zhan, R. and Percival, I.G. 2019. The end-Ordovician mass extinction: a single-pulse event? *Earth-Science Reviews*, 192, 15–33, https://doi.org/10. 1016/j.earscirev.2019.01.023
- Wignall, P.B. 2015. The Worst of Times: How Life on Earth Survived Eighty Million Years of Extinction. Princeton University Press.
- Williams, S.H. 1988. Dob's Linn the Ordovician–Silurian boundary stratotype. Bulletin of the British Museum, Natural History: Geology, 43, 17–30.
- Yan, D., Chen, D., Wang, Z., Li, J., Yang, X. and Zhang, B. 2019. Climatic and oceanic controlled deposition of Late Ordovician–Early Silurian black shales on the North Yangtze platform, South China. *Marine and Petroleum Geology*, 110, 112–121, https://doi.org/10.1016/j.marpetgeo.2019.06.040
- Young, S.A., Saltzman, M.R., Ausich, W.I., Desrochers, A. and Kaljo, D. 2010. Did changes in atmospheric CO₂ coincide with latest Ordovician glacial-interglacial cycles? *Palaeogeography, Palaeoclimatology, Palaeoecology*, 296, 376–388, https://doi.org/10.1016/j.palaeo.2010.02.033

- Young, S.A., Edwards, C.T., Ainsaar, L., Lindskog, A. and Saltzman, M.R. 2023. Seawater signatures of Ordovician climate and environment. *Geological Society, London, Special Publications*, 532, 137–156, https://doi.org/10.1144/SP532-2022-258
- Zhang, B., Yao, S. et al. 2020. Middle Permian organic carbon isotope stratigraphy and the origin of the Kamura Event. Gondwana Research, 79, 217–232, https://doi.org/10.1016/j.gr.2019.09.013
- Zhang, T., Shen, Y., Zhan, R., Shen, S. and Chen, X. 2009. Large perturbations of the carbon and sulfur cycle associated with the Late Ordovician mass extinction in South China. *Geology*, 37, 299–302, https://doi.org/10.1130/G25477A.1
- Zheng, Y., Anderson, R.F., van Geen, A. and Kuwabara, J. 2000. Authigenic molybdenum formation in marine sediments: a link to pore water sulfide in the Santa Barbara Basin. *Geochimica et Cosmochimica Acta*, 64, 4165–4178, https://doi.org/10.1016/S0016-7037(00)00495-6
- Zheng, Y., Anderson, R.F., van Geen, A. and Fleisher, M.Q. 2002. Preservation of particulate non-lithogenic uranium in marine sediments. *Geochimica et Cosmochimica Acta*, 66, 3085–3092, https://doi.org/10.1016/S0016-7037(01) 00632-9
- Zhou, L., Wignall, P.B., Su, J., Feng, Q., Xie, S., Zhao, L. and Huang, J. 2012. U/Mo ratios and $\delta^{98/95}$ Mo as local and global redox proxies during mass extinction events. *Chemical Geology*, **324–325**, 99–107, https://doi.org/10.1016/j.chemgeo.2012.03.020
- Zhou, L., Algeo, T.J. *et al.* 2015. Changes in marine productivity and redox conditions during the Late Ordovician Hirnantian glaciation. *Palaeogeography, Palaeoclimatology, Palaeoecology,* **420**, 223–234, https://doi.org/10.1016/j.palaeo.2014.12.012
- Zirks, E., Krom, M. et al. 2021. Redox evolution and the development of oxygen minimum zones in the Eastern Mediterranean Levantine basin during the early Holocene. Geochimica et Cosmochimica Acta, 297, 82–100, https://doi.org/ 10.1016/j.gca.2021.01.009
- Zou, C., Qiu, Z., Wei, H., Dong, D. and Lu, B. 2018a. Euxinia caused the Late Ordovician extinction: evidence from pyrite morphology and pyritic sulfur isotopic composition in the Yangtze area, South China. *Palaeogeography*, *Palaeoclimatology*, *Palaeoecology*, 511, 1–11, https://doi.org/10.1016/j. palaeo.2017.11.033
- Zou, C., Qiu, Z. et al. 2018b. Ocean euxinia and climate change 'double whammy' drove the Late Ordovician mass extinction. Geology, 46, 535–538, https://doi.org/10.1130/G40121.1